Health condition monitoring of insulated joints based on axle box acceleration measurements

Molodova, Maria; Oregui Echeverria-Berreyarza, Maider; Nunez Vicencio, Alfredo; Li, Zili; Dollevoet, Rolf

DOI
10.1016/j.engstruct.2016.05.018

Publication date
2016

Document Version
Accepted author manuscript

Published in
Engineering Structures

Citation (APA)
Molodova, M., Oregui Echeverria-Berreyarza, M., Nunez Vicencio, A., Li, Z., & Dollevoet, R. (2016). Health condition monitoring of insulated joints based on axle box acceleration measurements. *Engineering Structures*, *123*(September), 225-235. https://doi.org/10.1016/j.engstruct.2016.05.018

Please cite as: M. Molodova, M. Oregui, A. Núñez, Z. Li, and R. Dollevoet, "Health condition monitoring of insulated joints based on axle box acceleration measurements". Engineering Structures, Volume 123, Issue 2016, September 2016, Pages: 225-235. DOI: 10.1016/j.engstruct.2016.05.018

Health Condition Monitoring of Insulated Joints based on Axle Box Acceleration Measurements

Maria Molodova, Maider Oregui, Alfredo Núñez, Zili Li*, and Rolf Dollevoet

Section of Railway Engineering, Faculty of Civil Engineering and Geosciences, Delft University of Technology, Stevinweg 1, 2628 CN Delft, The Netherlands

*Corresponding author:
Zili Li
tel: +31 15 27 82325;
fax: +31 15 27 83443;
email: Z.Li@tudelft.nl;
address: Section of Railway Engineering, Faculty of Civil Engineering and Geosciences, Delft University of Technology, Stevinweg 1, 2628 CN Delft, The Netherlands.

Abstract

This paper presents a health condition monitoring system for insulated rail joints (IRJs) based on axle box acceleration (ABA) measurements. The ABA signals from all the wheels of the measuring train are processed to extract those characteristics that better represent the quality of the IRJ. Then, different indicators are used for damage assessment, the most relevant being a set of frequency bands in the ABA power spectrum. A detection algorithm is proposed based on the derived frequency characteristics of the ABA signal. We compared the responses of IRJs in good condition with those in poor condition. Track inspections were performed to validate the health condition monitoring methodology in different IRJs of the Dutch railway network. The hit rate of IRJs detection was 84% for two validated tracks. The damage assessment procedure allowed to prioritize the IRJs that require maintenance. This information is useful for the railway inframanagers as it allows to predict where safety compromises will be faced.

Keywords: Railway infrastructure monitoring, insulated joints, axle box acceleration measurements, damage detection.

1. Introduction

Insulated Rail Joints (IRJs) are critical components in the railways infrastructure as they are the core of signalling systems, in which the railway network is divided into electrically isolated sections of tracks. When a train is running over a section, a short circuit is created and the signalling system switches from green to red, indicating that the track is occupied. Thus, the failure of IRJs affects the safety of the railways, because the malfunction of the signalling system can lead into a severe accident. Consequently, maintenance measures should be taken if an IRJ is found in a bad condition. In a late stage of degradation, these measures are expensive and time consuming because usually the IRJ has to be replaced. Moreover, the maintenance measures are carried out up to 5 times more frequently at an IRJ

Please cite as: M. Molodova, M. Oregui, A. Núñez, Z. Li, and R. Dollevoet, "Health condition monitoring of insulated joints based on axle box acceleration measurements". Engineering Structures, Volume 123, Issue 2016, September 2016, Pages: 225-235. DOI: 10.1016/j.engstruct.2016.05.018

than at other track components (Pang and Dhanasekar, 2006) as IRJs are a weak link in the track structure.

An IRJ constitutes a discontinuity to the track, see Figure 1. The rail ends are connected with two joint bars, placed on both sides of the rail web, and the gap between the rail ends is filled with an isolating component called endpost. The joint bars are attached to the rails by bolts and epoxy adhesive. The IRJs are characterized by high impact dynamic forces at the wheel/rail interface (Wen et al., 2005), caused by the combination of two factors: lower bending stiffness of the joint bars comparing to that of the rail, leading to larger deflection (Jenkins et al., 1974; Kerr and Cox, 1999); and lower values of the Young's modulus of the endpost comparing to the one of the steel (Chen and Kuang, 2002). The impact dynamic forces may have several consequences on the state of an IRJ, such as the resulting high stress concentration producing plastic deformation of the rail surface (Kabo et al., 2006); "cavity-like" damage appearing in the rail head after the gap (Sandstrom et al., 2012); the high maximum shear stress leading to the partial loss of the bond between the joint bars and the rail (Himebaugh et al., 2008), and the contribution to the growth of cracks starting from the holes in the rail (Mayville and Stringfellow, 1995).

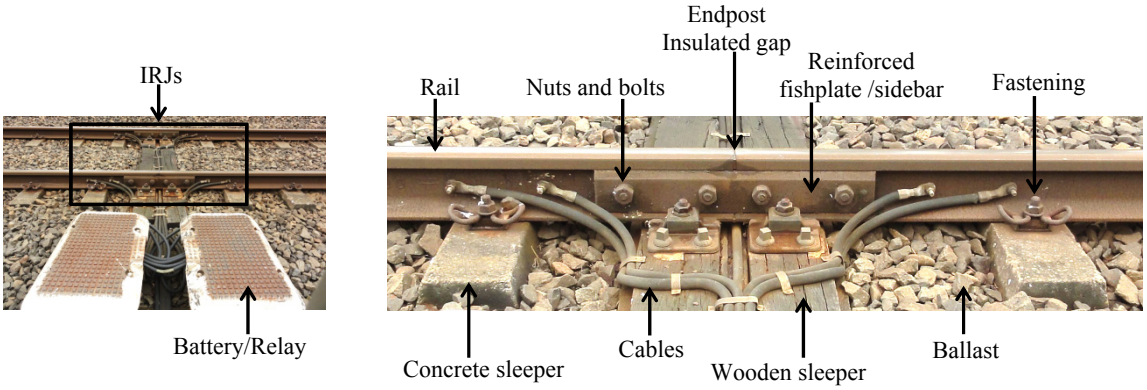

Figure 1: Picture of an IRJ and its main components.

The existing studies have focused on understanding the influence of vehicle and track components on the degradation of IRJs to eliminate or lighten the dynamic response between the wheel and the track (Jenkins et al., 1974; Mayville and Stringfellow, 1995; Wu and Thompson, 2003; Pang and Dhanasekar, 2006; Davis and Akhtar, 2007; Himebaugh et al. 2008; Li et al., 2008; Sandstrom and Ekberg, 2009; Dhanasekar and Bayissa, 2012, Mandal and Dhanasekar, 2013, Mandal, 2014a, Mandal, 2014b). The speed of the train has a significant effect on the wheel/rail contact forces (Jenkins et al., 1974; Wen et al., 2005). For tracks, the misalignment between the rail ends at a joint and the track parameters that increase the flexibility of the IRJ are the most important factors (Wu and Thompson, 2003; Plaut et al., 2007; Himebaugh et al. 2008; Li et al., 2008; Zong et al., 2013).

Currently, the monitoring of the IRJs health condition is mainly based on visual inspection (Yella et al., 2009), which is dangerous for the operators and the resulting assessment may contain subjectivity introduced by the human factors. Visual inspections are supplemented with eddy current (Oukhellou et al., 2008) and ultrasound measurements (Brizuela et al., 2011) for detection of cracks. However, some conditions of IRJs can still not be detected by these three methods. For example, the cracks in the rail web hidden by the joint bars can only be detected at a late stage when the immediate replacement of the IRJ is the only possible

Please cite as: M. Molodova, M. Oregui, A. Núñez, Z. Li, and R. Dollevoet, "Health condition monitoring of insulated joints based on axle box acceleration measurements". Engineering Structures, Volume 123, Issue 2016, September 2016, Pages: 225-235. DOI: 10.1016/j.engstruct.2016.05.018

measure. Another example is the partial loss of the bond between the joint bars and the rail which may be the beginning of the mechanical failure (Davis and Akhtar, 2005) or an electrical failure as water can get in and short-circuit the two rail ends.

In this paper, we propose an on-train automatic health condition monitoring system using axle box acceleration (ABA) to monitor the condition of IRJs. The advantage of the ABA method comparing to eddy current and ultrasonic techniques is that ABA is related to the contact force in the wheel-rail interface, and hence, represents the dynamic impact interaction between wheel and rail at an IRJ. High dynamic responses observed in ABA can be a measure of degradation states of IRJ that cannot be assessed with ultrasound and eddy-current measurements, like plastics deformation without cracks, hidden or very small cracks, loose bolts, etc. In view that the ABA system can detect track defects such as corrugation, welds of poor quality and squats, and assess different deterioration states (Molodova et al., 2014a), we believe that the condition of IRJs can be monitored, as the impact is significantly higher at IRJs than at short track defects. The other important advantage of the ABA system is that the measurements are performed on-board of a running vehicle, minimizing both the hours of unavailable track due to maintenance and the number of visual inspections required, while the condition of each IRJ is assessed by an automatic decision algorithm.

The process of the health condition monitoring of IRJs with the ABA method includes the detection of the location of the IRJ in the ABA data and subsequent damage classification and assessment. The general methodology of the detection of short track defects was described in Molodova et al., 2014a; however, in the case of IRJs the characteristic frequencies and deterioration analysis is different than those of short wavelength defects. The main focus of the present paper is the analysis of different damage states of IRJs based on ABA measurements to assess the IRJs health condition.

To investigate the applicability of the ABA measurements to the health condition monitoring of IRJs, a set of real-life IRJs is assessed for two tracks in the Netherlands. IRJs in different conditions are included in the study, such as IRJs in a good state or with visible surface degradation at different states, IRJ with a crack in the fastener, and with damaged insulation layer. The degradation state of IRJs is validated based on the photos taken on the track site. The ABA responses at those IRJs are analysed in both the time and the frequency domains, including frequencies up to 1400 Hz. Based on the results, different indicators are defined to classify the IRJ conditions, where the most relevant are certain frequencies of the ABA signal.

The paper is divided as follows. In Section 2, the theoretical background of the health condition monitoring of IRJs using ABA measurements is discussed. In Section 3, the damaged-IRJ analyses based on ABA and the hammer test are presented. In Section 4, the results of the automatic detection of IRJs are provided and the guidelines for the assessment of the health condition of IRJs are outlined.

2. Health condition monitoring of IRJs using ABA measurements

2.1 ABA measurement system

The ABA measurements were performed on board of a measuring train using a patented ABA technology (Li and Molodova, 2011). The sensitivity of ABA to rail profile deviation was investigated in Li et al., 2015. It has been shown that even trivial rail surface indentations of 10 mm long and 0.05 – 0.2 mm deep can be effectively detected by the ABA technology.

Please cite as: M. Molodova, M. Oregui, A. Núñez, Z. Li, and R. Dollevoet, "Health condition monitoring of insulated joints based on axle box acceleration measurements". Engineering Structures, Volume 123, Issue 2016, September 2016, Pages: 225-235. DOI: 10.1016/j.engstruct.2016.05.018

The ABA was measured by general purpose accelerometers mounted on the axle boxes of the wheels. Figure 2 represents a scheme of the whole system IRJ – train. The full set of acceleration measurements for the train *i* are in the vector $a_i(t)$. The recorded data also included the GPS coordinates $x_i(t)$ and the train speed $v_i(t)$ which was around the normal operational speed of the measuring train (100 km/h). The full measurement vector is denoted as $y_i(t)$, $y_i(t)=[a_i(t)\ x_i(t)\ v_i(t)]$.

Figure 2: Track conditions are assessed via signal processing methods using on-board measurements.

2.2 Health condition monitoring of IRJs

The health condition of the railway infrastructure is a distributed parameter system, which is dependent on various factors in both temporal and spatial domain. For instance, the health of an IRJ will be influenced temporally by the tonnage of the trains passing over, but also by the local conditions of sleepers, ballast, fastenings, etc.

Let us represent the health condition of an IRJ located at x_j as $H\left(t,x_j\right)\in\Im$. This function can only take values within a discrete set $\Im=\left\{N,D_1,D_2,...,D_K\right\}$.

The IRJ at time *t* can be in a healthy condition *N*, or it can present a certain type of degradation D_k, with $k=1,..,K$ among a set of possible conditions. In this paper, we study three types of IRJ's degradation: the plastic deformation of the rail surface after the gap (D_1), damaged fastener (D_2), and damage of the insulation layer (D_3).

By using the measurements $y_i(t)$, the health condition monitoring system should be able to estimate $H(t,x_j)$ for the whole set of IRJs of the track. Two main characteristics of ABA are analysed in this paper. The first one is the local maximum ABA due to the impact at IRJ *j*:

$$a_j^{\max}=\max_{t_j\le t\le t_j+\Delta t}a_i\left(t\right) \tag{1}$$

where t_j is the instant when the train is passing by at the discontinuity of the IRJ *j*: $x_i(t_j)=x_j$ and Δt is a reasonable time for allowing the visualization of the full response of the IRJs. In this paper, Δt is the time that the train needs to travel the distance between the gap and the end of

Please cite as: M. Molodova, M. Oregui, A. Núñez, Z. Li, and R. Dollevoet, "Health condition monitoring of insulated joints based on axle box acceleration measurements". Engineering Structures, Volume 123, Issue 2016, September 2016, Pages: 225-235. DOI: 10.1016/j.engstruct.2016.05.018

the joint bar, around 340 mm, that is $x_i\left(t_j\right)-x_i\left(t_j+\Delta t\right)\approx 340$. To determine t_j a detection algorithm of IRJs is presented in section 2.4.

The second characteristic is the power spectrum density (PSD) of the ABA signal $P_{a_i a_i}\left(f\right)$, which can be obtained for finite time-series $a_i[m]$ as follows:

$$P_{a_i a_i}\left(f\right)=\frac{1}{T}\left(\frac{\Delta t}{M-1}\right)^2\left\|\sum_{m=1}^{M}a_i\left[m\right]e^{-j2\pi fm}\right\|^2 \tag{2}$$

with M the length of the vector $a_i[m]$, and using the sampled ABA signal at discrete times given by the resolution of the sensor, starting from the instant t_j (the moment of impact with the IRJ) until the axle box of the train reached the end of the joint bar at around 340 mm after the impact (denoted as $t_j+\Delta t$). Thus, the discrete series is defined as $a_i\left[m\right]=a_i\left(t_j+\left(m-1\right)\frac{\Delta t}{M-1}\right)$, for a total measurement period $T=\Delta t$.

Then, by using a_j^{max} and $P_{a_i a_i}\left(f\right)$ in the frequency range $f\in\left[0,1400\right]Hz$, an estimation $\hat{H}\left(t,x_j\right)$ of the health condition of the IRJ j is proposed in this paper. As the inputs for this estimation come from an automated ABA measuring system, the health condition of the IRJs can be automatically monitored as well.

In the next sections, the automatic detection algorithm of IRJ based on the wavelet analysis of the ABA signals is presented. Then, to enable the automatic damage assessment of IRJs, the ABA signals at IRJs of different quality $\left\{D_1,D_2,D_3\right\}$ are analysed for an estimation of the relationships between the health of IRJs and ABA characteristics, such as the maximum ABA magnitude a_j^{max} and the PSD $P_{a_i a_i}\left(f\right)$. The process of the IRJ's health condition monitoring is displayed in Figure 3.

Please cite as: M. Molodova, M. Oregui, A. Núñez, Z. Li, and R. Dollevoet, "Health condition monitoring of insulated joints based on axle box acceleration measurements". Engineering Structures, Volume 123, Issue 2016, September 2016, Pages: 225-235. DOI: 10.1016/j.engstruct.2016.05.018

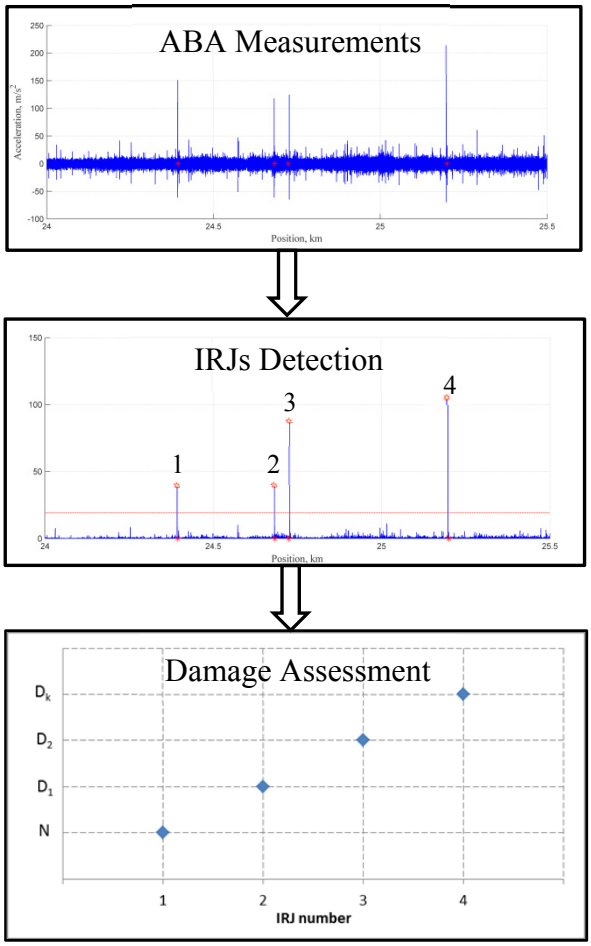

Figure 3: The health condition monitoring scheme of the IRJs.

2.3 Wavelet power spectrum

In this section we present the wavelet-based detection algorithm for identification of IRJs' locations in the ABA signal. Since the IRJs cause local variations in the frequency spectrum of ABA signals, they can be detected by the wavelet analysis, namely continuous wavelet transform (CWT) (Liew and Wang, 1998; Wang and Deng, 1999; Ovanesova and Suárez, 2004). CWT is a time-frequency analysis tool in which the observed function (such as ABA) is multiplied by a group of shifted and scaled wavelet functions. If a_m denotes the ABA signals, and ψ a mother wavelet function, then CWT can be defined as follows (Daubechies, 1990):

$$W_m(s) = \sum_{m'=0}^{M-1} a_{m'} \psi^* \left(\frac{(m'-m)\delta_t}{s} \right) \tag{3}$$

where $W_m(s)$ are wavelet coefficients, δ_t is a time step of ABA signal, m is the time index, $m'=0,...M-1$ is the time shift operator, $\psi^* \left(\frac{(m'-m)\delta_t}{s} \right)$ is a family of wavelets deduced from the mother wavelet by translations and scaling, * indicates a complex conjugate, and s is

Please cite as: M. Molodova, M. Oregui, A. Núñez, Z. Li, and R. Dollevoet, "Health condition monitoring of insulated joints based on axle box acceleration measurements". Engineering Structures, Volume 123, Issue 2016, September 2016, Pages: 225-235. DOI: 10.1016/j.engstruct.2016.05.018

a wavelet scale, $s>0$. In this paper we used the Morlet function as a mother wavelet, defined as follows:

$$\psi_0(\eta) = \pi^{-1/4} e^{i\omega_0\eta} e^{-\eta^2/2} \tag{4}$$

where ω_0 is a non-dimensional frequency. The wavelet power spectrum (WPS) is defined as the square of the wavelet coefficients:

$$\left|W_m^2(s)\right| \tag{5}$$

In order to facilitate the signal processing for detection, a one dimensional signal, i.e. scale averaged wavelet power, that captures the important frequencies is defined in the next section.

2.4 Scale averaged wavelet power

Wavelet analysis has been effectively employed for automatic detection of squats (Molodova et al., 2014a). With some adjustments of the detection parameters, this method can also be employed for detection of IRJs. The automatic detection algorithm is based on the scale averaged wavelet power (SAWP), which measures the localized variations of wavelet power spectrum in certain frequency bands.

SAWP is defined as the weighted sum of squared wavelet coefficients over scales s_{j1} to s_{j2} (Torrence and Compo, 1998):

$$\overline{W}_m^2 = \frac{\delta j \delta t}{C_\delta} \sum_{j=j_1}^{j_2} \frac{\left|W_m(s_j)\right|^2}{s_j}, \tag{6}$$

where δj is a scale step, δt is time step, C_δ is an empirically derived constant for each wavelet function.

For detection of IRJs, SAWP can be calculated in a certain frequency band related to IRJs. Then, by finding the local maxima of SAWP, which exceed an empirical threshold, the damaged IRJs can be detected.

The detection rate of damaged IRJs is evaluated in terms of hit rate and false alarm rate. The hit rate is calculated as the ratio of the number of correct prediction and the total number of damaged IRJs in the investigated track section. The false alarm rate is defined as the ratio of the number of false alarms and the total number of predictions. For accurate detection hit rate should be maximized and false alarm rate should be minimized. Moreover, when GPS and tachometer signals are also used, a robust detection can be guaranteed.

3. Damage assessment

To determine the major temporal (a_j^{max}) and frequency characteristics ($P_{a_i a_i}(f)$) related to various damage states of IRJs, the ABA measurements at IRJs were investigated in the two tracks with different substructure properties, Eindhoven – Weert and Groningen – Assen in the Netherlands. The damage states of the IRJs included in the study were plastic deformation

Please cite as: M. Molodova, M. Oregui, A. Núñez, Z. Li, and R. Dollevoet, "Health condition monitoring of insulated joints based on axle box acceleration measurements". Engineering Structures, Volume 123, Issue 2016, September 2016, Pages: 225-235. DOI: 10.1016/j.engstruct.2016.05.018

of the rail surface after the gap $H\left(t,x_j\right)=D_1$, cracks in the fastener $H\left(t,x_j\right)=D_2$, and damage to the insulation material $H\left(t,x_j\right)=D_3$.

3.1 Local maximum ABA

The IRJs are usually characterized by high values of ABA. In Figure 4, we relate the local maximum ABA to the state of the IRJ from the two tracks. The photos of some of the IRJs of Figure 4 are presented in Figure 5. The ABA signals from repeated measurement runs were low-pass filtered with the cut-off frequency of 2 kHz, to include the frequency range typically excited at short wave track defects (Molodova et al. 2014b). The blue circles in Figure 4 are the average local maximum of six repeated signals on the track Eindhoven – Weert (Figure 4*a*), and four repeated signals on the track Groningen – Assen (Figure 4*b*); the range of ABA maximum values was indicated by the grey diamonds.

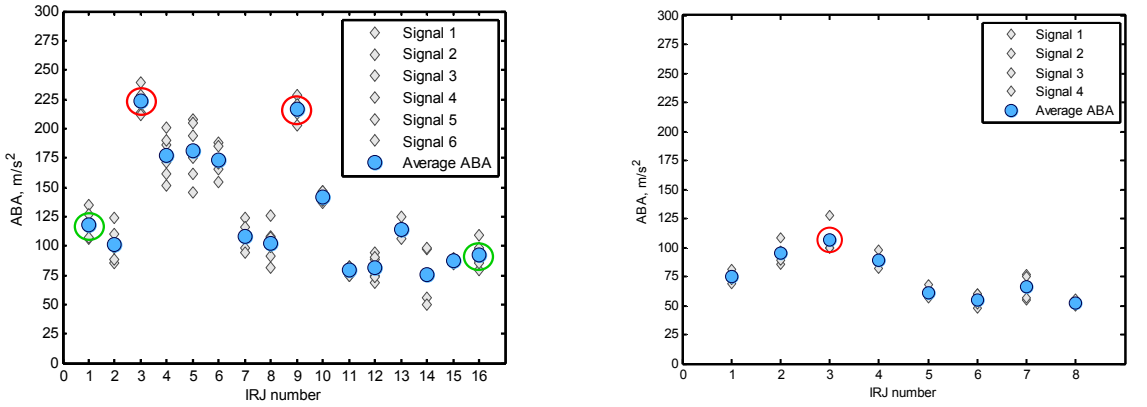

(a) Track Eindhoven – Weert in 2010 *(b) Track Groningen – Assen in 2010*

Figure 4: Local maxima of ABA at IRJs. Blue circles indicate average local maxima, grey diamonds denotes the maximum of each ABA measurement.

To study the relationships between the state of IRJs and ABA values we compared two IRJ with high ABA magnitude (IRJs number 3 and number 9 indicated with red circles in Figure 4*a*) and two IRJs with comparatively low ABA magnitude (IRJs number 1 and number 16 indicated with green circles in Figure 4*a*). As it appeared from the visual inspection of the IRJs, the two IRJs with high ABA magnitudes (above 200 m/s^2) were indeed in a deteriorated condition: the IRJ number 3 had plastic deformation D_1 on the rail surface caused by the impact at the endpost (Figure 5*c*) and the IRJ number 9 had a crack in the fastener D_2 (Figure 5*g-h*). As for the IRJs with comparatively low ABA magnitude (below 150 m/s^2), the IRJ number 1 may be considered as in a good condition (Figure 5*a*), since only light deformation of the rail surface is visible. While the IRJ number 16 had a significant gap between the two pieces of the rail, as a result of the loss of insulation material D_3 (Figure 5*j*). Thus, the ABA magnitude at IRJs cannot be an indication of D_3. Therefore, further investigation of the frequency content of ABA is presented in the next section.

Please cite as: M. Molodova, M. Oregui, A. Núñez, Z. Li, and R. Dollevoet, “Health condition monitoring of insulated joints based on axle box acceleration measurements”. Engineering Structures, Volume 123, Issue 2016, September 2016, Pages: 225-235. DOI: 10.1016/j.engstruct.2016.05.018

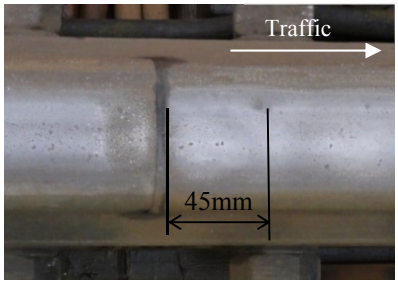

(a) IRJ number 1 with light surface deformation.

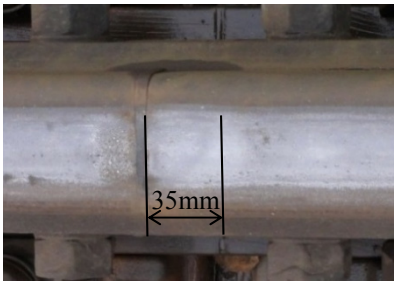

(b) IRJ number 2 with light surface deformation.

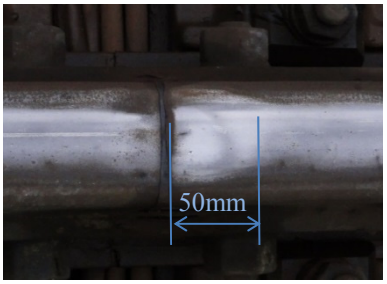

(c) IRJ number 3 with severe plastic deformation.

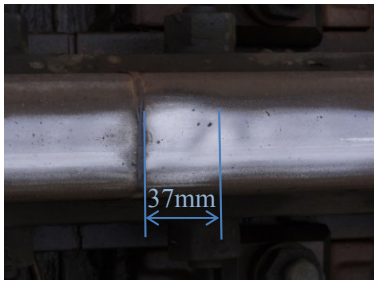

(d) IRJ number 4 with severe plastic deformation.

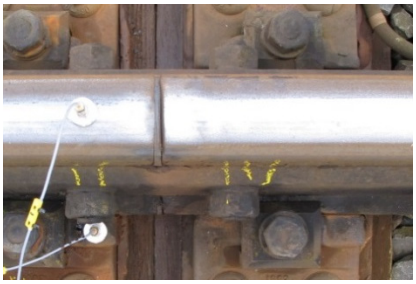

(e) IRJ number 7 with rusty fastening.

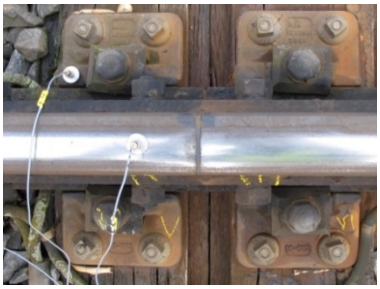

(f) IRJ number 8 with rusty fastening.

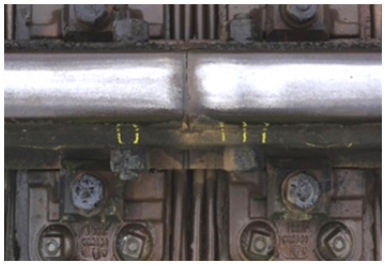

(g) IRJ number 9 with a crack in the fastener.

(h) IRJ number 9 with a crack in the fastener, side view.

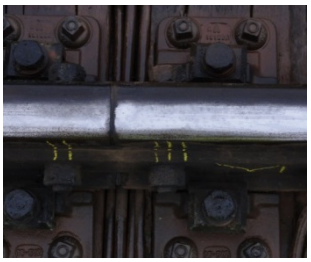

(i) IJ number 10

(j) IRJ number 16 with damaged insulation layer and a crack in the fastener.

(k) IRJ number 16 with damaged insulation layer and a crack in the fastener.

(l) IRJ number 3 on the track Groningen – Assen.

Figure 5: Photos of IRJs in 2010. The photos (*a*)-(*k*) are on the track Eindhoven – Weert with the numbering of IRJ corresponding to Figure 8*a* and the photo (*l*) is on the track Groningen – Assen. The traffic direction in these photos is from left to right.

Please cite as: M. Molodova, M. Oregui, A. Núñez, Z. Li, and R. Dollevoet, "Health condition monitoring of insulated joints based on axle box acceleration measurements". Engineering Structures, Volume 123, Issue 2016, September 2016, Pages: 225-235. DOI: 10.1016/j.engstruct.2016.05.018

In Figure 4*b* the ABA on the track Groningen – Assen has less variation in values, than on the track Eindhoven – Weert, with the average local maxima ranging between 50 to 100 m/s^2. The IRJ with the highest ABA value is number 3, which has moderate degradation of the rail surface D_1 (Figure 5*l*).

3.2 Damage analysis based on ABA

In this section the analysis of the frequency content at the IRJs is presented. The study is based on the six IRJs on the track Eindhoven – Weert (four IRJs with plastic deformation, one with fastener damage and one with damaged insulation layer), and one IRJ on the track Groningen – Assen, with light plastic deformation.

Plastic deformation on the rail surface

In this section, four IRJs from the track Eindhoven – Weert (E-W) were investigated, IRJ number 1 and 2 with light plastic deformation (Figure 5*a*-*b*) and the IRJ number 3 and 4 with severe plastic deformation of the rail surface (Figure 5*c*-*d*). The plastic deformation is caused by the impact occurring after the gap and has a typical wavelength of about 35-50 mm (Oregui et al, 2015b). Since IRJ number 2 with light surface deformation did not have any other visible damage at the fastener and insulation layer, it will also be used for comparison in the next sections as a reference IRJ in normal condition.

The ABA measured at these four IRJs are shown in Figure 6*a*. The ABA signals for each IRJ in this section and the next sections are the average signals out of four repetitive ABA signals, filtered with the low-pass Butterworth filter with a cut-off frequency of 2 kHz. The averaging and the filtering were done in order to reduce the noise in the measured signals. The ABA signals at these IRJs had a wavelength of about 50 mm. The local maximum ABA was the highest for IRJ number 3 ($a_{D_1}^{max}$ = 220 m/s^2) and about 2.4 times higher than ABA at the IRJ number 2 in normal condition (a_N^{max} = 91 m/s^2). The plastic deformation at IRJ number 3 has the longest wavelength among these four IRJ's, 50 mm (Figure 5*c*).

The PSD at these IRJs is shown in Figure 6*b*. The major peaks for the IRJs fall into the following frequency ranges: 70 – 170 Hz, 270 – 350 Hz and 500 – 550 Hz. The largest peak is at 520 Hz for IRJ number 4 with severe rail surface plastic deformation. The peak that appears in each ABA signal in the frequency range between 500 Hz and 550 Hz might be related to the plastic deformation of the rail surface. As the train speed was 100 km/h the vibrations in the range of 500 – 550 Hz are related to the wavelength of the wave pattern of 50 – 55 mm of the rail surface. When the wave pattern on the rail surface starts to develop, the vibrations in the range of 500 – 550 Hz work as a positive feedback mechanism. That is, the wave pattern of 50 – 55 mm increases the vibrations at 500 – 550 Hz, and higher level of vibrations at this frequency causes further plastic deformation with a wavelength of 50 – 55 mm.

IRJ number 3 has the longest wavelength of plastic deformation (50 mm) and the highest local maximum ABA compared to the other three IRJs in Figure 6a. However, the PSD at 500-550 Hz for IRJ number 3 was not the highest among these IRJs, because the energy was distributed over a range of frequencies (270 Hz, 730 Hz, 830 Hz, 1150 Hz, see Figure 6*b*). This can indicate that there is damage in other components of IRJ number 3 besides plastic deformation of the rail surface (sleeper, fastener, etc.) Thus, there is no direct correlation between degree of plastic deformation of the rail surface and PSD at 500-550 Hz. However, the combination of high ABA magnitudes and high values of PSD at 500-550 Hz can

Please cite as: M. Molodova, M. Oregui, A. Núñez, Z. Li, and R. Dollevoet, "Health condition monitoring of insulated joints based on axle box acceleration measurements". Engineering Structures, Volume 123, Issue 2016, September 2016, Pages: 225-235. DOI: 10.1016/j.engstruct.2016.05.018

qualitatively indicate the plastic deformation. For this reason in Section 4.2 we use both ABA magnitude and PSD to make a conclusion about damage state.

Figure 6*c* presents the ABA measured at IRJs 3 from the track Groningen – Assen (G-A), see photo in Figure 5*l*. The ABA signal at this IRJs had a wavelength of about 50 mm. The local maximum ABA was $a_{D_1}^{max} = 100$ m/s^2, which is quite close to the normal condition ($a_N^{max} = 91$ m/s^2). The PSD at these IRJs is shown in Figure 6*d*. There major peaks for this IRJ are 90 Hz, 350 Hz and 570 Hz, which is consistent with the frequencies in Figure 6*b*.

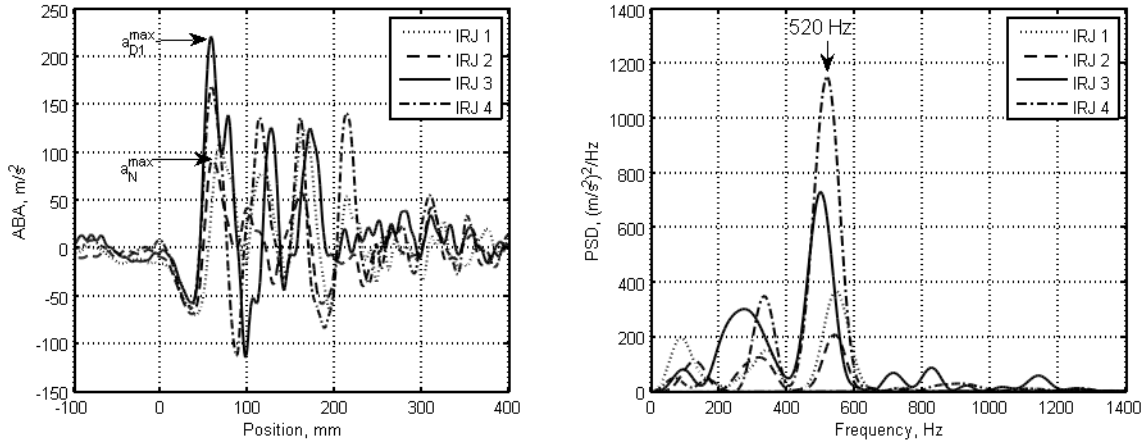

(a) ABA at IRJs with plastic deformation (E-W) *(b) PSD at IRJs with plastic deformation (E-W)*

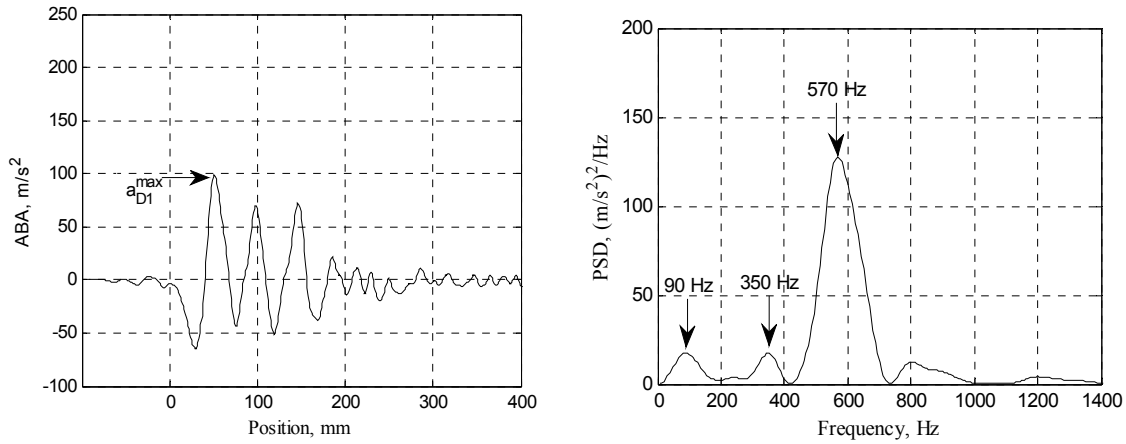

(c) ABA at IRJs with plastic deformation (G-A) *(d) PSD at IRJs with plastic deformation (G-A)*

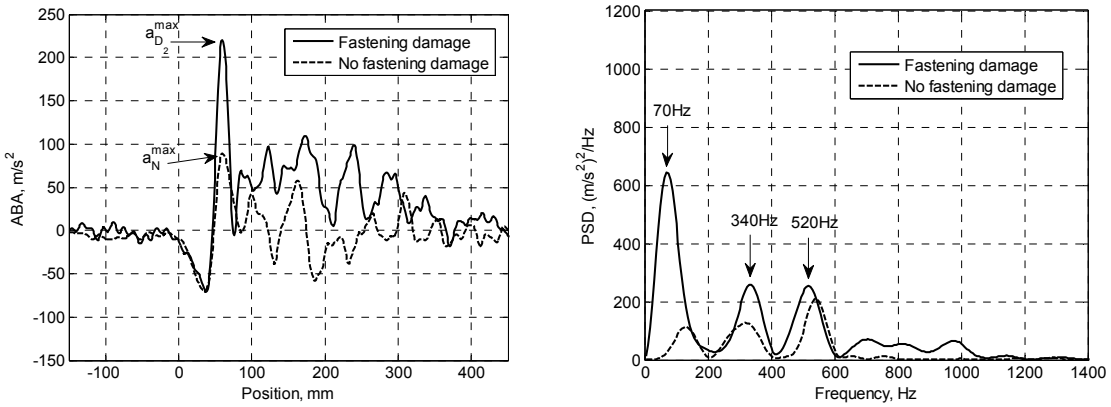

(e) ABA at an IRJ with a crack in the fastener (E-W) *(f) PSD at an IRJ with a crack in the fastener (E-W)*

Figure 6: ABA and PSD at various IRJs, October 2010

Please cite as: M. Molodova, M. Oregui, A. Núñez, Z. Li, and R. Dollevoet, "Health condition monitoring of insulated joints based on axle box acceleration measurements". Engineering Structures, Volume 123, Issue 2016, September 2016, Pages: 225-235. DOI: 10.1016/j.engstruct.2016.05.018

Damage of fastener

In this section the IRJ with a crack in the fastener was investigated (D_2). That is IRJ number 9 in Figure 5*g*-*h*. The dynamic responses at this IRJ were compared to the reference IRJ without visible damage in the fastener (Figure 5*b*).

The ABA at the IRJ with a crack in the fastener is shown in Figure 6*e* (solid line) together with the reference IRJ (dashed line). The ABA signal at this IRJ has a high peak of about $a_{D_2}^{max}$=220 m/s^2. This peak is also related to high contact force, which caused the deformation of the rail surface, visible in Figure 5*g* as a broadened shiny wavy running band after the gap. It can also be observed in Figure 6*e* that the ABA magnitude of the IRJ number 9 is elevated compared to the reference one.

The PSD at the IRJ with a crack in the fastener is presented in Figure 6*f*. The major peak for an IRJ with a crack in the fastener is at 70 Hz, and the other two peaks at 340 Hz and 520 Hz are similar to the peaks of the reference IRJ. The frequency at 70 Hz is probably related to the change in the stiffness of the fastening caused by the crack. This frequency might be responsible for the higher level of vibration after the gap.

Damage of insulation layer

In this section, an IRJ number 16 with two types of damage was investigated: with damaged insulation layer (Figure 5*j*) and the crack in the fastener (Figure 5*k*). The damage of the fastener for this IRJ was similar to the one of IRJ number 9 in Figure 5*h*.

The ABA at this IRJ is shown in Figure 7*a* with a solid line. The ABA magnitude at this IRJ is comparable to the reference IRJ ($a_{D_3}^{max}$=86 m/s^2), but the wavelength is shorter than that of the reference signal. The PSD at the IRJ with the damaged insulation layer is shown in Figure 7*b*. The major two frequencies for this IRJ are 100 Hz and 645 Hz.

From these data it is impossible to extract the information about the health state of the IRJ due to low ABA magnitude and PSD. Thus, the retrospective analysis of the ABA measurements was performed to obtain more information. Figure 7*c* presents the ABA signals measured in October 2009 – July 2010. The ABA magnitude at this IRJ in October 2009 was $a_{D_3}^{max}$=134 m/s^2, in March 2010 was $a_{D_3}^{max}$=129 m/s^2, and in July 2010 was $a_{D_3}^{max}$=257 m/s^2.

The major two frequencies in the PSD for this IRJ are 100 Hz and 540 Hz (Figure 7*d*). The frequency of 100 Hz is close to the frequency of 70 Hz obtained by the analysis of Figure 6*f* and must be related to the crack in the fastener. As for the damage of the insulation layer, it was difficult to see in these data any specific features related to this phenomenon.

Please cite as: M. Molodova, M. Oregui, A. Núñez, Z. Li, and R. Dollevoet, "Health condition monitoring of insulated joints based on axle box acceleration measurements". Engineering Structures, Volume 123, Issue 2016, September 2016, Pages: 225-235. DOI: 10.1016/j.engstruct.2016.05.018

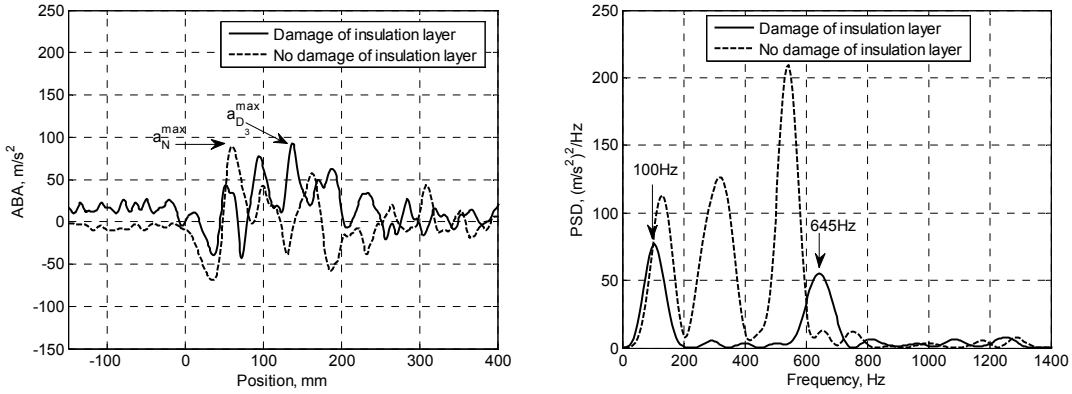

(a) ABA at an IRJ with damaged insulation layer (2010)(b) PSD at an IRJ with damaged insulation layer(2010)

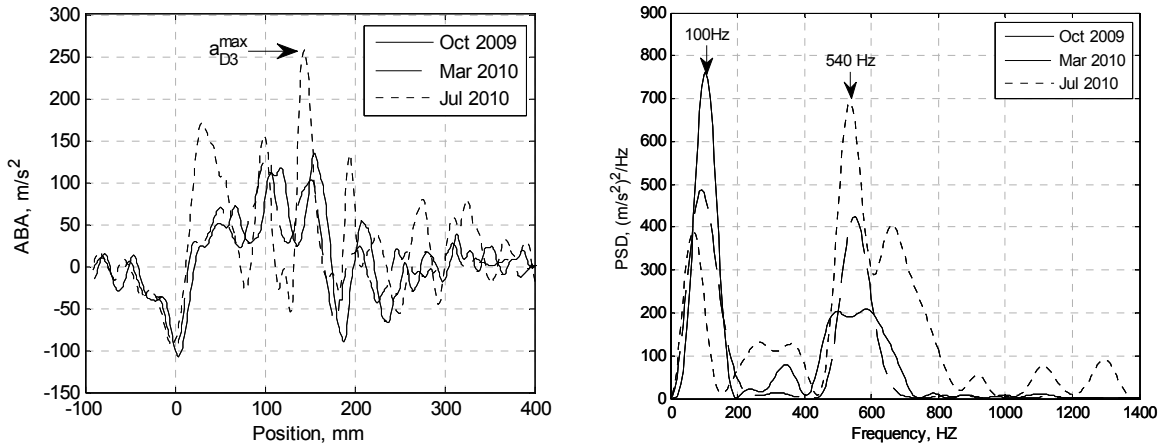

(c) ABA trends at an IRJ with damaged insulation layer (d) PSD trends at an IRJ with damaged insulation layer

Figure 7: ABA and PSD at an IRJ with damaged insulation layer, track Eindhoven - Weert.

3.3 Damaged-IRJ analysis based on hammer test

Hammer test measurements are widely used to characterize the dynamic behaviour of railway tracks (S.L. Grassie et al., 1982; M. Hiensch et al., 2002; M. Oregui et al., 2015a). By examining the frequency response measured via the hammer test, insight into the condition of the track can be gained (A. Remennikov and S. Kaewunruen, 2006; S. Kaewunruen and A. M. Remennikov, 2008; M. Molodova et al., 2014b; M. Molodova et al., 2014c). A schematic representation of the hammer test is shown in Figure 8. During the hammer test the rail is excited with a hammer and the track response is measured with accelerometers at the location of interest. The excitation force is measured with a force sensor. The measurement configuration in this study included the response measured with a unidirectional accelerometer placed on the top of the rail above the third bolt (Figure 8) and vertical excitation of the rail close to the measurement location.

Please cite as: M. Molodova, M. Oregui, A. Núñez, Z. Li, and R. Dollevoet, "Health condition monitoring of insulated joints based on axle box acceleration measurements". Engineering Structures, Volume 123, Issue 2016, September 2016, Pages: 225-235. DOI: 10.1016/j.engstruct.2016.05.018

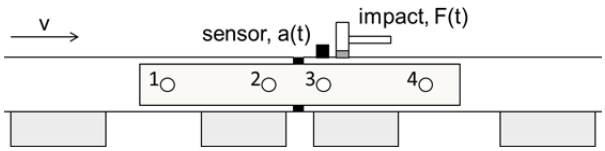

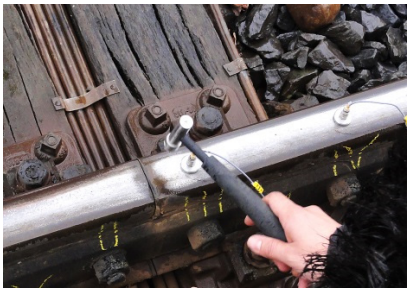

(a) A scheme of the hammer test measurement configuration *(b) A photo of the hammer test*

Figure 8: The hammer test measurement configuration on an IRJ.

In order to reduce noise in the measured data, the rail was excited five times. Then, the average force *F(t)* and acceleration *a(t)* were calculated over the five consecutive signals. The averaged force and acceleration signals were transformed into the frequency domain by fast Fourier transform and the receptance function of the IRJ *j*, $R_j(f)$, was calculated as follows:

$$R_j(f) = \frac{1}{(2\pi f)^2}\frac{S_{aF}(f)}{S_{FF}(f)} = \frac{1}{(2\pi f)^2}\frac{\sum_{n=1}^{N}\sum_{m=1}^{N-m-1} a[m+n]F[m]e^{-j2\pi fn}}{\sum_{n=1}^{N}\sum_{m=1}^{N-m-1} F[m+n]F[m]e^{-j2\pi fn}} \quad (3)$$

where *f* is frequency, S_{aF} is the cross-spectrum between the force and the acceleration, and S_{FF} is the autospectrum of the force. The frequency range of the receptance function is defined by the hammers used and the applicability of the measured data, which in this case, cover frequencies between 50 and 1200 Hz (M. Oregui et al., 2015a).

The receptance functions show the response of IRJs to vibrations in terms of displacement over force as a function of vibration frequencies. Thus, the characteristic resonances and anti-resonances of the track system can be identified. If differences are found in the health condition of the IRJs, differences are then expected between the corresponding frequency response functions. The goal of this analysis is to see whether these differences in the receptance functions agree with the differences found in the PSD functions examined in section 4.2.

Figure 9 presents the calculated receptance functions of the nominal and damaged IRJs studied in Section 4.2. For the IRJ with light surface deformation the following peaks were observed: 190 Hz, 350, 430 Hz, 560 Hz, 730 Hz, 900 Hz and 1006 Hz. Some of them (190 Hz, 350 Hz, and 560 Hz) agree with the results from the ABA analysis. For the IRJ with severe plastic deformation, there are peaks at 80 Hz, 190, 250 and 570 Hz that agree well with the results from the ABA measurements. The other two peaks, at 350 Hz and 1006 were not clearly observed in the ABA measurements. For the IRJ with a crack in the fastener the peaks in the receptance function were at about 50 Hz, 190 Hz, 270 Hz, 420 Hz, 580 Hz and 1045 Hz. The peak at about 50 Hz agrees with the major peak at 70 Hz from the ABA analysis; the peaks at about 270 Hz and about 580 Hz correspond more or less to the peaks observed in the ABA at 340 Hz and 520 Hz. The major peaks observed in the receptance function for the IRJ with a damaged insulation layer were at 107 Hz, 250 Hz, 370 Hz, 703 Hz and 1055 Hz. The

Please cite as: M. Molodova, M. Oregui, A. Núñez, Z. Li, and R. Dollevoet, "Health condition monitoring of insulated joints based on axle box acceleration measurements". Engineering Structures, Volume 123, Issue 2016, September 2016, Pages: 225-235. DOI: 10.1016/j.engstruct.2016.05.018

peaks at 107 Hz and 703 Hz agree with those at 100 Hz and 645 Hz observed in the ABA analysis.

In conclusion, most of the frequency characteristics found from ABA analysis were also observed in the hammer test (with some deviation, due to the different loading conditions and some random factors). The hammer test revealed some frequency characteristics that were not measured using ABA. These were probably filtered out by the wheel.

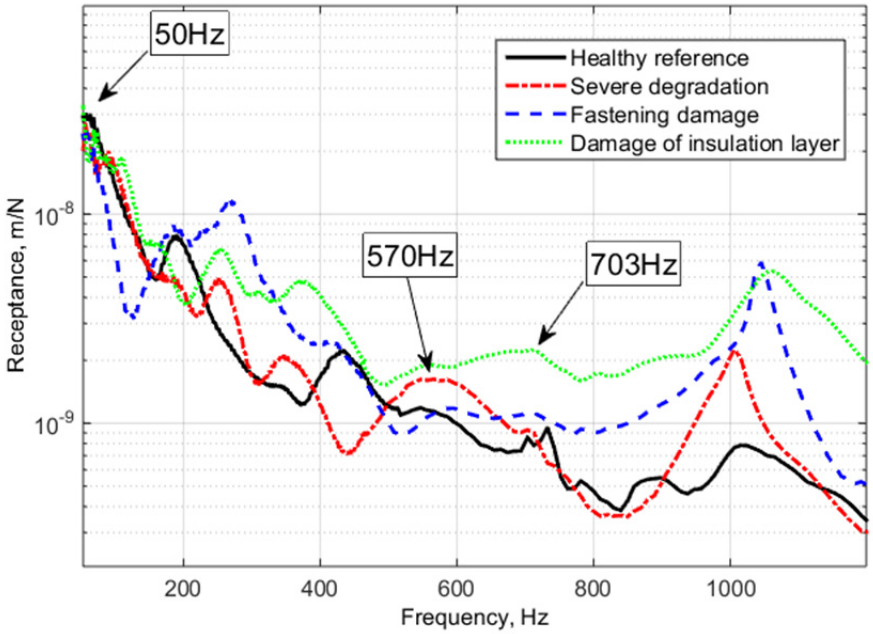

Figure 9: Receptance functions at the investigated IRJs.

4. Summary of the experimental results

4.1 Detection of IRJs

In order to improve the hit rate of the IRJs, the pre-processing of the measured data has to be performed. Since the major frequencies related to IRJs lies below 1200 Hz, the ABA signals were filtered with a low-pass Butterworth filter with a cut-off frequency of 1200 Hz and normalized by the standard deviation. The ABA measured on the track Eindhoven – Weert of 24 km long with 75 locations of IRJs was used to run the detection.

Figure 10*a*-*b* shows the calculated SAWP functions for right and left rails on a section of this track with 8 IRJ's locations, marked with red asterisks. The detection resulted in 77 predicted locations, with 62 of them being correct; 13 locations have been missed and 15 locations were falsely predicted. The hit rate of this detection is 83% and the false alarm rate is 19%.

Figure 10*c*-*d* presents the prediction for another track, Groningen – Assen. The length of the investigated track was 2.2 km with 4 IRJ's locations in total. One of the IRJs at position -62.5km on the left rail was missed by the automatic detection. However, this location was detected from the signal on the other rail, and thus, by combination of the signals from both rails all the IRJs can be detected. In Figure 10c there is also one rail defect at -63.160 km.

Please cite as: M. Molodova, M. Oregui, A. Núñez, Z. Li, and R. Dollevoet, “Health condition monitoring of insulated joints based on axle box acceleration measurements”. Engineering Structures, Volume 123, Issue 2016, September 2016, Pages: 225-235. DOI: 10.1016/j.engstruct.2016.05.018

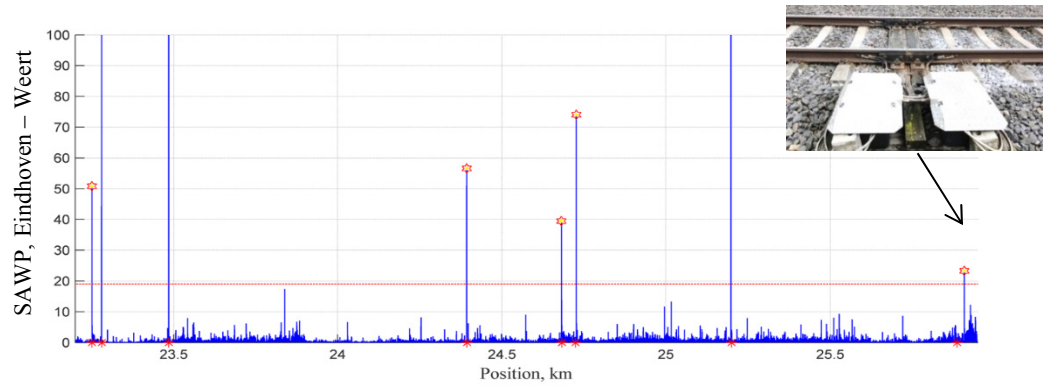

(a) Track Eindhoven – Weert, right rail

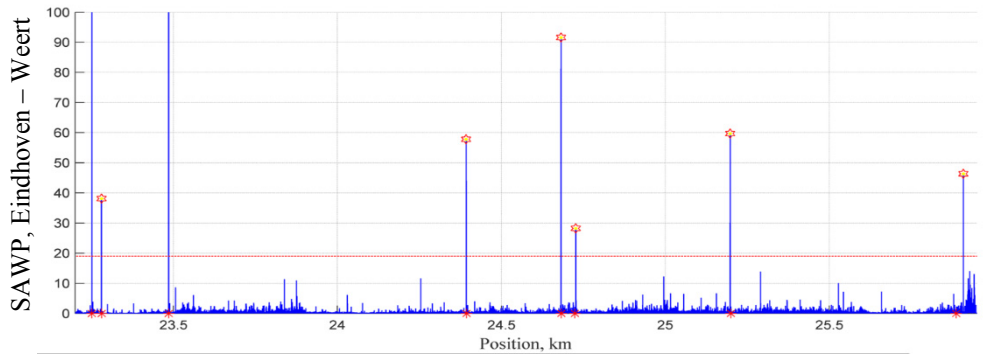

(b) Track Eindhoven – Weert, left rail

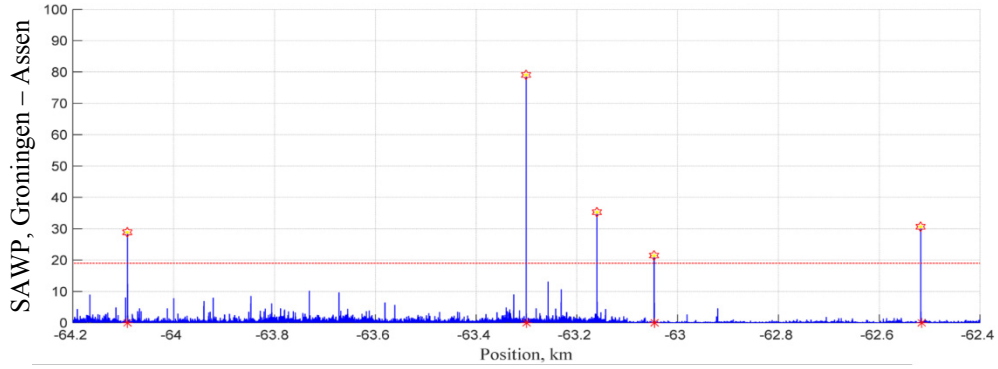

(c) Track Groningen – Assen, right rail

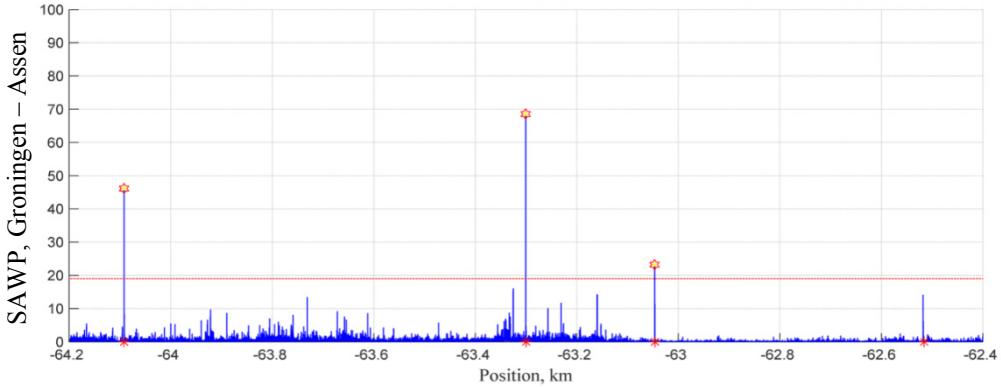

(d) Track Groningen – Assen, left rail

Figure 10: Detection of IRJs.

Please cite as: M. Molodova, M. Oregui, A. Núñez, Z. Li, and R. Dollevoet, "Health condition monitoring of insulated joints based on axle box acceleration measurements". Engineering Structures, Volume 123, Issue 2016, September 2016, Pages: 225-235. DOI: 10.1016/j.engstruct.2016.05.018

which was falsely detected as an IRJ. This is an artificial rail surface defect, which was made for another research (Molodova et al., 2014b) by removing a thin layer of the material on the rail head. Since this artificial defect is an unusual situation on the rail, it can be excluded from our investigation, and we can conclude that the false alarm rate is zero for this track. The combined hit rate of detection from the two tracks is 84% with the false alarm rate 19%.

Track	Number of IRJs (T)	Number of predictions (P)	Number of correct predictions (H)	Number of false alarms (F)	Hit rate (H/T)	False Alarms (F/P)
Eindhoven - Weert	75	77	62	15	83%	19%
Groningen - Assen	4	4	4	0	100%	0%
Total	79	81	66	15	**84%**	**19%**

Table 1: Hit rate of IRJs detection.

4.2 Assessment of IRJs health condition

When the locations of the IRJs are detected, the assessment of the IRJs health condition can be performed based on the damage-IRJ analysis presented in section 4. The normal health condition is characterized by low ABA magnitude (a_N^{max}<100 m/s^2) and low PSD values ($P_{a_N a_N}([70;100]) < 200$ (m/s^2)^2/Hz, $P_{a_N a_N}([520;570]) < 400$ (m/s^2)^2/Hz). The IRJs with sever plastic deformation of the rail surface are characterized by high ABA values (a_{D1}^{max}>100 m/s^2), and high PSD values around 520 – 570 Hz ($P_{a_{D_1} a_{D_1}}([520;570]) > 400$ (m/s^2)^2/Hz). The IRJs with fastener damage are characterized by high ABA values ($a_{D_2}^{max}$>100 m/s^2), and high PSD values around 70 – 100 Hz ($P_{a_{D_2} a_{D_2}}([70;100]) > 200$ (m/s^2)^2/Hz).

Figure 11 presents the assessment of IRJs health condition for the two tracks. The normal health condition is denoted by *N*, the plastic deformation of the rail surface after the gap is denoted by D_1, the fastener damage is denoted by D_2, and the uncertain health condition is denoted by D_k. The results presented in Figure 11 agree with the observation of the IRJs health conditions in Figure 5. Further investigation of various health conditions of IRJs is needed in order to improve these results and assess the IRJ with uncertain health conditions. The health conditions D_1, D_2 and D_k indicate that deterioration of the IRJ has started and it is recommended to the inframanager to increase the frequency of inspections to prevent the failure of the IRJ. The proposed assessment can be used as performance indicator (Stenström et al., 2015), in order to simplify the overall analysis. The methodology can facilitate the maintenance operations providing crucial information that can be used to optimally design a condition based inspection plan strategy (Uzarski and Grussing, 2013) and maintenance decision making under risk averse situations (Rockafellar and Royset, 2015).

Please cite as: M. Molodova, M. Oregui, A. Núñez, Z. Li, and R. Dollevoet, "Health condition monitoring of insulated joints based on axle box acceleration measurements". Engineering Structures, Volume 123, Issue 2016, September 2016, Pages: 225-235. DOI: 10.1016/j.engstruct.2016.05.018

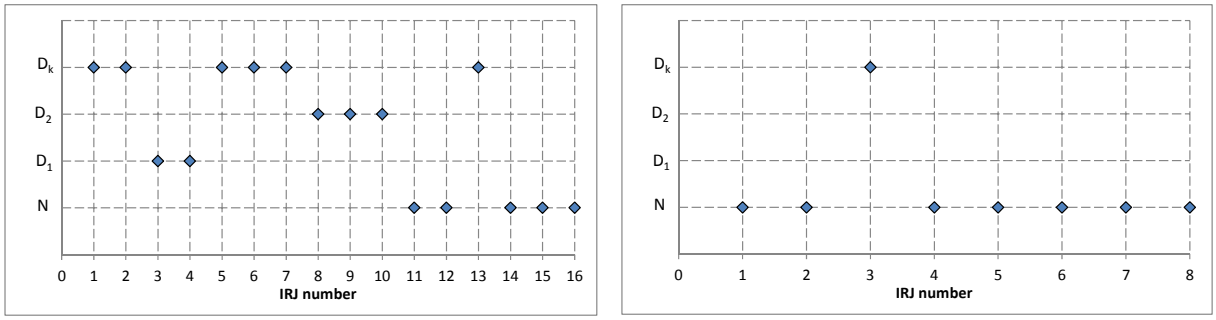

(a) Track Eindhoven – Weert *(b) Track Groningen - Assen*

Figure 11: Assessment of IRJs health condition: N – normal condition, D_1 – plastic deformation, D_2 – fastener damage, D_k – the health condition is uncertain.

5. Conclusions and further research

In this paper an ABA health condition monitoring system for IRJ was presented. First, the automatic detection algorithm for identification of the locations of interest was proposed. The hit rate of detection of the IRJs was 84% for two Dutch tracks, with 19% false alarm rate.

To study the applicability of the ABA system to the health monitoring of IRJs, the conditions of a set of real-life IRJs were assessed for different tracks in the Netherlands. IRJs of different quality were included in the study, such as with joints in good condition or with visible surface degradation of varying degrees, IRJs with cracks in the fastener and IRJs with a damaged insulation layer. The degradation state was assessed based on photos. Subsequently, the ABA responses were analysed in the time and frequency domains. Based on the results, different indicators were defined to classify the conditions of the IRJs, of which the most relevant were certain characteristic frequencies related to the different types of IRJ damages. The proposed indicators were verified using hammer tests.

Elaboration of the health condition assessment algorithm of IRJs is part of future work. For example, the quantitative relations presented in this paper can be further developed for predicting the degree of degradation of IRJs, based on broader real-life data as well as theoretical analysis, e.g. numerical simulations. Further, the remaining life of IRJ can be assessed by the ABA method. For example, in case of detection of an IRJ with damaged insulation layer, the maintenance action should be an immediate repair of the IRJ, as insufficient insulation may cause faults in the signalling system, leading to a severe accident. In case of detection of an IRJ with broken fastener, the fastener should be replaced. The remaining life of the IRJ after the replacement of the fastener depends on the degree of degradation of other components of the IRJ. In case of detection of an IRJ with plastic deformation, timely grinding can be an effective way to treat it, unless the degradation is too severe. Moreover, the internal cracks can be present in the rail, significantly reducing the remaining life of the IRJ. These issues should be further investigated to relate the degree of degradation to the remaining life of the IRJ.

The application of the results of this study to the health monitoring of IRJs will increase the safety of the railway network and reduce the total yearly IRJ replacement cost by including intelligent preventive maintenance strategies employing the information gathered by this health monitoring system.

Please cite as: M. Molodova, M. Oregui, A. Núñez, Z. Li, and R. Dollevoet, "Health condition monitoring of insulated joints based on axle box acceleration measurements". Engineering Structures, Volume 123, Issue 2016, September 2016, Pages: 225-235. DOI: 10.1016/j.engstruct.2016.05.018

Acknowledgments

This research is part of the STW/ProRail project "Detection and Diagnosis of Railway Track Short Wave Anomalies (DrTrack)", number 12246. The Dutch Technology Foundation STW is part of the Netherlands Organisation for Scientific Research (NWO), and is partly funded by the Ministry of Economic Affairs. Also, this research was supported by the Basque Government of Spain (Grant No. BFI10), and by the Dutch railway infrastructure manager ProRail.

References

J. Brizuela, C. Fritsch, and A. Ibáñez, 2011. "Railway wheel-flat detection and measurement by ultrasound", Transportation Research Part C: Emerging Technologies 19(6), pp. 975-984. DOI: 10.1016/j.trc.2011.04.004

Y. Chen and J. Kuang, 2002. "Contact stress variations near the insulated rail joints", Proceedings of the Institution of Mechanical Engineers, Part F: Journal of Rail and Rapid Transit 216(4), pp. 265-274. DOI: 10.1243/095440902321029217

I. Daubechies, 1990. "The wavelet transform, time-frequency localization and signal analysis," IEEE Transactions on Information Theory, 36(5), pp. 961-1005. DOI: 10.1109/18.57199

D. Davis and M. Akhtar, 2007. "Improved insulated rail joints for high tonnage lines with heavy-axle loads", Railway Track and Structures 103(8), pp. 24-29.

D. Davis and M. Akhtar, 2005. "Improving the performance of bonded insulated joints", Railway Track and Structures 101(1), pp. 14-17.

M. Dhanasekar and W. Bayissa, 2012. "Performance of square and inclined insulated rail joints based on field strain measurements", Proceedings of the Institution of Mechanical Engineers, Part F: Journal of Rail and Rapid Transit, vol. 226 no. 2 pp.140-154. DOI: 10.1177/0954409711415898

S.L. Grassie, R.W. Gregory, D. Harrison, and K.L. Johnson, 1982. "The dynamic response of railway track to high frequency vertical excitation", Journal of Mechanical Engineering Science 24, pp. 77-90. DOI: 10.1243/JMES_JOUR_1982_024_016_02

M. Hiensch, J.C.O. Nielsen, and E. Verheijen, 2002. "Rail corrugation in the Netherlands - Measurements and simulations", Wear 253, pp. 140-149. DOI: 10.1016/S0043-1648(02)00093-5

A. Himebaugh, R. Plaut, and D. Dillard, 2008. "Finite element analysis of bonded insulated rail joints", International Journal of Adhesion and Adhesives 28(3), pp.142-150. DOI: 10.1016/j.ijadhadh.2007.09.003

H. Jenkins, J. Stephenson, G. Clayton, G. Morland, and D. Lyon, 1974. "The effect of track and vehicle parameters on wheel/rail vertical dynamic forces", Railway Engineering Journal 3(1), pp. 2-16.

E. Kabo, J. Nielsen, and A. Ekberg, 2006. "Prediction of dynamic train-track interaction and subsequent material deterioration in the presence of insulated rail joints", Vehicle System Dynamics 44 (SUPPL. 1), pp. 718-729. DOI: 10.1080/00423110600885715

S. Kaewunruen and A. M. Remennikov, 2008. "An alternative rail pad tester for measuring dynamic properties of rail pads under large preloads", Experimental Mechanics 48, pp. 55-64. DOI: 10.1007/s11340-007-9059-3

A. Kerr and J. Cox, 1999. "Analysis and tests of bonded insulated rail joints subjected to vertical wheel loads", International Journal of Mechanical Sciences 41(10), pp. 1253-1272. DOI: 10.1016/S0020-7403(98)00042-3

Z. Li, X. Zhao, C. Esveld, R. Dollevoet, and M. Molodova, 2008. "An investigation into the causes of squats—Correlation analysis and numerical modeling," Wear, 265(9/10), pp. 1349–1355. DOI: 10.1016/j.wear.2008.02.037

Z. Li and M. Molodova, 2011. "Method and instrumentation for detection of rail defects, in particular rail top defects". European Patent, WO2011019273 (A1) — 2011-02-17.

Z. Li, X. Zhao, R. Dollevoet, and M. Molodova, 2008. "Differential wear and plastic deformation as causes of squat at track local stiffness change combined with other track short defects", Vehicle System Dynamics 46(SUPPL.1), pp. 237-246. DOI: 10.1080/00423110801935855

Z. Li, M. Molodova, A. Nunez, and R. Dollevoet, 2015. "Improvements in Axle Box Acceleration Measurements for the Detection of Light Squats in Railway Infrastructure," IEEE Transactions on Industrial Electronics, vol. 62, no. 7, pp. 4385–4397, Jul. 2015. DOI: 10.1109/TIE.2015.2389761

K.M. Liew and Q. Wang, 1998. "Application of wavelet theory for crack identification in structures," Journal of Engineering Mechanics, 124(2), pp. 152-157. DOI: 10.1061/(ASCE)0733-9399(1998)124:2(152)

N.K. Mandal, 2014a. "On the low cycle fatigue failure of insulated rail joints (IRJs)", Engineering Failure Analysis 40, pp. 58-74. DOI: 10.1016/j.engfailanal.2014.02.006

N. K. Mandal, M Dhanasekar and Y Q Sun, 2016. "Impact forces at dipped rail joints", Proceedings of the Institution of Mechanical Engineers, Part F: Journal of Rail and Rapid Transit 230(1), pp. 271-282. DOI: 10.1177/0954409714537816

N.K. Mandal and M. Dhanasekar, 2013. "Sub-modelling for the ratchetting failure of insulated rail joints", International Journal of Mechanical Sciences, 75, pp. 110-122. ISSN 0020-7403, DOI: 10.1016/j.ijmecsci.2013.06.003.

R.A. Mayville and R.G. Stringfellow, 1995. "Numerical analysis of a railroad bolt hole fracture problem", Theoretical and Applied Fracture Mechanics 24(1), pp. 1-12. DOI: 10.1016/0167-8442(95)00026-B

M. Molodova, Z. Li, A. Núñez, and R. Dollevoet, 2014a. "Automatic detection of squats in the railway infrastructures", IEEE Transactions on Intelligent Transportation Systems, 15(5), pp. 1980-1990. DOI: 10.1109/TITS.2014.2307955.

M. Molodova, Z. Li, A. Núñez, and R. Dollevoet, 2014b. "Validation of a finite element model for axle box acceleration at squats in the high frequency range", Computers and Structures 141(1), pp. 84-93. DOI: 10.1016/j.compstruc.2014.05.005

M. Molodova, Z. Li, A. Núñez, and R. Dollevoet, 2015. "Parameter study of the axle box acceleration at squats". Proceedings of the Institution of Mechanical Engineers Part F: Journal of Rail and Rapid Transit 229(8), pp. 841-851. DOI:10.1177/0954409714523583

M. Oregui, Z. Li, and R. Dollevoet, 2015a. "Identification of characteristic frequencies of damaged railway tracks using field hammer test measurements", Mechanical Systems and Signal Processing, 54(1), pp.224-242. DOI: 10.1016/j.ymssp.2014.08.024

M. Oregui, M. Molodova, A. Núñez, R. Dollevoet, and Z. Li, 2015b. "Experimental Investigation into the Condition of Insulated Rail Joints by Impact Excitation," Experimental Mechanics, 55(9), pp. 1597-1612. DOI: 10.1007/s11340-015-0048-7

L. Oukhellou, E. Côme, L. Bouillaut, and P. Aknin, 2008. "Combined use of sensor data and structural knowledge processed by Bayesian network: Application to a railway diagnosis aid scheme", Transportation Research Part C: Emerging Technologies 16(6), pp. 755-767. DOI: 10.1016/j.trc.2008.04.001.

A.V. Ovanesova and L.E. Suárez, 2004. "Applications of wavelet transforms to damage detection in frame structures," Engineering Structures 26(1), pp. 39-49. DOI: 10.1016/j.engstruct.2003.08.009

T. Pang and M. Dhanasekar, 2006. "Dynamic finite element analysis of the wheel-rail interaction adjacent to the insulated rail joints", in Proceedings of the 7th International Conference on Contact Mechanics and Wear of Wheel/Rail System, 24-27 September, 2006, Brisbane, Australia.

R. Plaut, H. Lohse-Busch, A. Eckstein, S. Lambrecht, and D. Dillard, 2007. "Analysis of tapered, adhesively bonded, insulated rail joints", Proceedings of the Institution of Mechanical Engineers, Part F: Journal of Rail and Rapid Transit 221(2), pp. 195-204. DOI: 10.1243/0954409JRRT107

A. Remennikov and S. Kaewunruen, 2006. "Experimental investigation on dynamic railway sleeper/ballast interaction", Experimental Mechanics 46, pp. 57-66. DOI: 10.1007/s11340-006-5868-z

R.T. Rockafellar and J.O. Royset, 2015. "Engineering decisions under risk averseness", ASCE-ASME Journal of Risk and Uncertainty in Engineering Systems, Part A: Civil Engineering 1(2), paper number 04015003. DOI: 10.1061/AJRUA6.0000816.

J. Sandstrom, E. Kabo, A. Nissen, F. Jansson, A. Ekberg, and R. Lunden, 2012. "Deterioration of insulated rail joints - a three-year field study", in Proceedings of the 9th

International Conference on Contact Mechanics and Wear of Rail/Wheel Systems, pp. 301-308, Chengdu, China, 2012.

J. Sandstrom and A. Ekberg, 2009. “Numerical study of the mechanical deterioration of insulated rail joints”, Proceedings of the Institution of Mechanical Engineers, Part F: Journal of Rail and Rapid Transit 223(3), pp. 265-273. DOI: 10.1243/09544097JRRT243

C. Stenström, A. Parida, J. Lundberg and U. Kumar, 2015. “Development of an integrity index for benchmarking and monitoring rail infrastructure: application of composite indicators”, International Journal of Rail Transportation 3(2), pp. 61-80. DOI: 10.1080/23248378.2015.1015220

C. Torrence, G.P. Compo, 1998. “A practical guide to wavelet analysis”, Bulletin of the American Meteorological Society 79(1), pp. 61-78. DOI: 10.1175/1520-0477(1998)079<0061:APGTWA>2.0.CO;2

D.R. Uzarski , M.N. Grussing, 2013. “Beyond mandated track safety inspections using a mission-focused, knowledge-based approach”, International Journal of Rail Transportation 1(4), pp. 218-236. DOI: 10.1080/23248378.2013.836397

Q. Wang and X. Deng, 1999. “Damage detection with spatial wavelets,” International Journal of Solids and Structures 36(23), 3443-3468. DOI: 10.1016/S0020-7683(98)00152-8

Z. Wen, X. Tin, and W. Zhang, 2005. “Contact-impact stress analysis of rail joint region using the dynamic finite element method”, Wear 258(7-8), pp. 1301-1309. DOI: 10.1016/j.wear.2004.03.040

T. Wu and D. Thompson, 2003. “On the impact noise generation due to a wheel passing over rail joints”, Journal of Sound and Vibration 267(3), pp. 485-496. DOI: 10.1016/S0022-460X(03)00709-0

S. Yella, M. Dougherty, and N.K. Gupta, 2009. “Condition monitoring of wooden railway sleepers”, Transportation Research Part C: Emerging Technologies 17(1), pp. 38-55. DOI: doi:10.1016/j.trc.2008.06.002

N. Zong, H. Askarinejad, T. B. Heva, and M. Dhanasekar, 2013. “Service Condition of Railroad Corridors around the Insulated Rail Joints”, J. Transp. Eng. 139(6), pp. 643-650. http://dx.doi.org/10.1061/(ASCE)TE.1943-5436.0000541